Packet Waves in a Reaction-Diffusion System

Vladimir K. Vanag and Irving R. Epstein
Department of Chemistry and Volen Center for Complex Systems, MS 015, Brandeis University, Waltham, Massachusetts 02454-9110
(Received 30 October 2001; published 8 February 2002)

The finite-wavelength instability gives rise to a new type of wave in reaction-diffusion systems: packet waves, which propagate only within a wave packet, are found in experiments on the Belousov-Zhabotinsky reaction dispersed in water-in-oil AOT microemulsion (BZ-AOT) as well as in model simulations. Inwardly moving packet waves with negative curvature occur in experiments and in a model of the BZ-AOT system when the dispersion $d\omega_k/dk$ is negative at the characteristic wave number k_0. This result sheds light on the origin of antispirals.

DOI: 10.1103/PhysRevLett.88.088303 PACS numbers: 82.40.Ck, 02.70.Uu, 68.05.Gh, 82.33.Nq

Unraveling the mechanisms of nonequilibrium pattern formation is essential for understanding complex living and nonliving systems [1–3]. In general, pattern formation is associated with an instability of the homogeneous steady state. Instabilities may be classified on the basis of dispersion curves obtained by linear stability analysis [2]. Different values of the characteristic wave number k_0 and frequency ω_0 of the instability give rise to three fundamental types of patterns: Turing structures ($\omega_0 = 0, k_0 \neq 0$), which are periodic in space and stationary in time; homogeneous bulk oscillations (Hopf bifurcation, $\omega_0 = \omega_H \neq 0$ at $k_0 = 0$); and patterns periodic both in space and time (finite wavelength instability, $\omega_0 \neq 0$, $k_0 \neq 0$). The last type of instability may be subdivided into traveling waves and standing waves. Traveling waves in turn may be categorized as phase waves or trigger waves. Examples of trigger waves include outwardly rotating spiral waves (spirals) and concentric waves [4–6].

Recently, we have discovered new patterns: inwardly rotating spiral waves (antispirals) and inwardly propagating concentric waves (antipacemakers) [7]. These patterns were found in the Belousov-Zhabotinsky (BZ) reaction dispersed in water-in-oil aerosol OT (AOT) microemulsion. The BZ-AOT system [8,9] demonstrates a remarkable variety of patterns [10] as the volume fraction of water nanodroplets, ϕ_d, and the chemical composition are varied: Turing structures, standing waves, oscillatory clusters, accelerating waves, and a new wave phenomenon, which we identify here as *packet waves*. In this Letter we present these new experimental results, propose a simple model of the BZ-AOT system, and use this model to illuminate the mechanism of emergence of packet waves. We show that antisprials and antipacemakers are a special case of a more general phenomenon, inwardly moving packet waves.

The experimental arrangement and methods are described in detail elsewhere [7,10]. Patterns in a BZ-AOT microemulsion sandwiched between two flat optical windows, separated by an annular Teflon gasket of 2 cm inner diameter and 0.1 mm thickness, were observed at ambient temperature through a microscope equipped with a digital CCD camera. In Fig. 1a, packet waves propagate in the oscillatory medium parallel to the Teflon border close to the bottom left corner. Waves fail to propagate into the area to the right of and above the packet. Trigger waves in such a situation would propagate from one boundary to the other or until collision with another wave. After a few dozen periods of local oscillation, the wave packet is transformed into standing waves.

Figure 1b illustrates chaotic waves enveloped by plane waves (perpendicular to the arrow) that are unable to penetrate the oscillatory area at the top (the Teflon border is near the bottom). After 10–15 min, the chaotic waves evolve into waves that move in opposite directions in adjacent areas (Fig. 1c). Under other conditions, in which we also

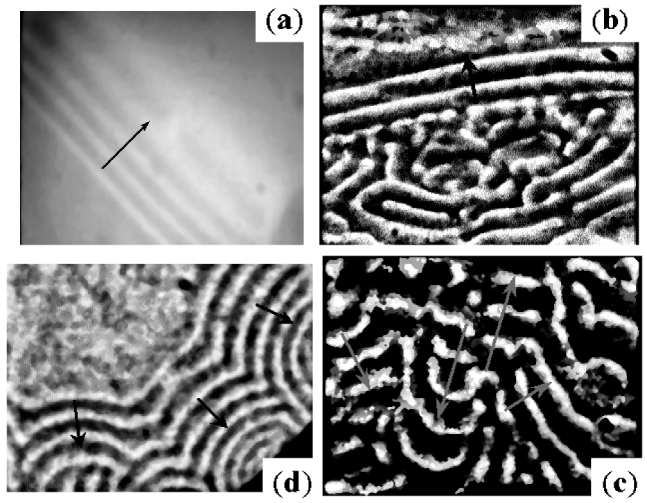

FIG. 1. Patterns in the BZ-AOT system. (a) $[H_2O]/[AOT] = 15$, (b),(c) $[H_2O]/[AOT] = 16.4$, (d) $[H_2O]/[AOT] = 15.2$. (a) $\phi_d = 0.57$, (b),(c) $\phi_d = 0.64$, (d) $\phi_d = 0.45$. (a) $[MA]/M = 0.25$, (b)–(d) $[MA]/M = 0.3$. (a),(d) $[H_2SO_4]/M = 0.2$, (b),(c) $[H_2SO_4]/M = 0.3$. (a) $[NaBrO_3] = 0.15$ M, (b),(c) $[NaBrO_3] = 0.2$ M, (d) $[NaBrO_3] = 0.23$ M. [ferroin] = 4 mM. (a) Size (mm × mm) = 2.5 × 2.2, (b),(c) size (mm × mm) = 1.88 × 1.4, (d) size (mm × mm) = 3.76 × 2.81. (c) Evolved from (b). White corresponds to the maximum value of catalyst Z (ferriin) concentration, black to minimum. Arrows mark direction of wave movement. Teflon border is seen in (d) at right bottom corner.

observed inwardly rotating spiral waves [7], we found waves moving toward the centers of their arcs, which were situated at the edge of the reaction area (Fig. 1d). These waves emerged at the boundary between the oscillatory area (left top corner) and the wave packet.

All the waves in Fig. 1 have a relatively small amplitude, much less than that of trigger waves or Turing structures, and exhibit roughly equal widths of the dark and bright stripes. We never observed a solitary propagating wave under the conditions of these experiments [ϕ_d near the percolation threshold (where the ratio of the diffusion coefficient of oil—soluble to that of water—soluble species is the largest) and chemical composition near the Hopf bifurcation].

Starting from a reduced form of the Oregonator model [11] of the BZ reaction, we have developed a four-variable model:

$$\partial x/\partial\tau = [x - x^2 - fz(x - q)/(x + q) - \beta x + s]/\varepsilon + D_x\Delta x\,, \quad (1)$$

$$\partial z/\partial\tau = x - z + \gamma u - \alpha z + D_z\Delta z\,, \quad (2)$$

$$\partial s/\partial\tau = (\beta x - s + \chi u)/\varepsilon_1 + D_s\Delta s\,, \quad (3)$$

$$\partial u/\partial\tau = (\alpha z - \gamma u)/\varepsilon_2 + D_u\Delta u\,, \quad (4)$$

where x and z are dimensionless concentrations of an activator ($HBrO_2$) and a catalyst (ferriin). If $\beta = \gamma = \alpha = 0$, Eqs. (1) and (2) reduce to the Oregonator model [11]; f and q are parameters, $q \ll 1$, and $1 < f < 3$. The additional variables, s and u, represent an inactive form of the activator (Br_2O_4) and Br_2, respectively, which are both soluble in the oil phase and diffuse rapidly: $D_s \gg D_x$, $D_u \gg D_z$, $D_u \cong D_s$, $D_x \cong D_z$. They may be thought of as providing a long-range positive and negative feedback, respectively. The species u produces s [χu term in Eq. (3)] via a chain of reactions ($Br_2 + MA \rightarrow Br^-$, $Br^- + Z \rightarrow Br^\bullet$, $Br_2 + MA^\bullet \rightarrow Br^\bullet$, $Br^\bullet + O_2 \rightarrow BrO_2{}^\bullet$, $BrO_2{}^\bullet + BrO_2{}^\bullet \rightarrow B_2O_4$). The corresponding term, $-\chi u$, is omitted from Eq. (4), since $\chi \ll \gamma$. Although there are no direct reactions that transform Br_2 (u) into catalyst (z) and *vice versa*, we introduced these reactions instead of the actual reactions, such as $Br_2 \leftrightarrow Br^-$, because the inhibitor Br^- is not explicitly included in our model, though its concentration, y, is proportional to z: $y = fz/(q + x)$ [11]. Parameters ε, ε_1, and ε_2 specify the ratios between the time scales of x, s, and u, respectively, and z.

We numerically integrated model (1)–(4) in the case of finite wavelength instability [the Jacobian matrix has two real, negative eigenvalues and one pair of complex eigenvalues λ_k with positive real part, $\mathrm{Re}(\lambda_k) \equiv a_k$, and nonzero imaginary part, $\mathrm{Im}(\lambda_k) \equiv \omega_k$, for some k, and a_k has a positive maximum at the characteristic wave number $k_0 \neq 0$] for the four combinations of the signs of a_k at $k = 0$ and $d\omega_k/dk$ at $k = k_0$ (see Fig. 2a): (a1) $a_k > 0$, $d\omega_k/dk > 0$, (b2) $a_k < 0$, $d\omega_k/dk > 0$, (c3) $a_k > 0$, $d\omega_k/dk < 0$, and (d4) $a_k < 0$, $d\omega_k/dk < 0$.

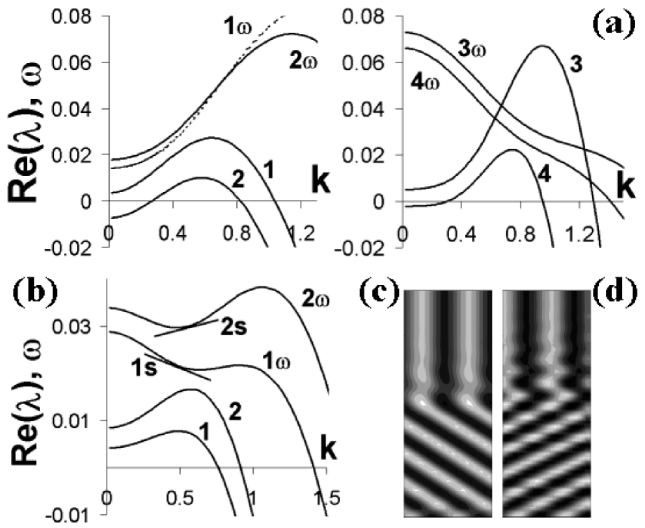

FIG. 2. Dispersion curves for model (1)–(4) (a),(b). (a) Curves 1–4 (real parts) and 1ω–4ω (imaginary parts) correspond to cases (a1), (b2), (c3), and (d4), respectively. Curves 1ω–4ω are shifted down by 0.97, 0.92, 1.245, and 1.17, respectively. Curves 3 and 4 are multiplied by 5. Parameters: (a1)–(c3) $D_x = D_z = 0.01$, (d4) $D_x = D_z = 0.015$; (a1),(b2),(d4) $D_u = D_s = 1$, (c3) $D_u = D_s = 0.9$; (a1),(b2) $q = 0.0015$, (c3),(d4) $q = 0.0033$; (a1),(b2) $f = 1.4$, (c3),(d4) $f = 1.5$; (a1) $\varepsilon = 0.34$, (b2) $\varepsilon = 0.36$, (c3) $\varepsilon = 0.4$, (d4) $\varepsilon = 0.385$; (a1),(b2) $\varepsilon_1 = 1.4$, (c3) $\varepsilon_1 = 3.5$, (d4) $\varepsilon_1 = 3.2$; (a1),(b2) $\varepsilon_2 = 0.006$, (c3) $\varepsilon_2 = 0.0016$, (d4) $\varepsilon_2 = 0.0024$; (a1) $\alpha = 6$, (b2) $\alpha = 7$, (c3) $\alpha = 6.2$, (d4) $\alpha = 6.3$; (a1),(b2) $\beta = 0.32$ (c3) $\beta = 0.28$, (d4) $\beta = 0.275$; (a1),(b2) $\gamma = 0.2$, (c3),(d4) $\gamma = 0.1$; (a1),(b2) $\chi = 0$, (c3) $\chi = 0.005\,95$, (d4) $\chi = 0.004$. (b) $q = 0.0033$, $f = 1.5$, (1) $\varepsilon = 0.297$, (2) $\varepsilon = 0.3$, $\varepsilon_1 = 2.1$, $\varepsilon_2 = 0.003$, (1) $\alpha = 10$, (2) $\alpha = 11$, $\beta = 0.29$, $\gamma = 0.1$, (1) $\chi = 0.000\,252$, (2) $\chi = 0.000\,21$, $D_x = D_z = 0.012$, (1) $D_u = 0.85$, (2) $D_u = 0.7$, $D_s = 1$. Curves 1ω and 2ω (imaginary parts) are shifted down by 1.155 and 1.125, respectively. Lines $1s$ and $2s$ show slope ($d\omega/dk$) at k_0. (c),(d) Space-time plots ($\Delta t = 10$, length = 100) after initial transient period t_0 for cases 1 and 2, respectively, shown in (b). 1D simulations initiated with local perturbation at one end (no-flux boundary conditions) at $t = 0$, $t_0 = 2000$ for (c) and $t_0 = 1000$ for (d).

Outwardly propagating packet waves (moving away from the perturbed region) were found whenever $d\omega_k/dk > 0$ (Fig. 3) for any type of initial perturbation (single point, narrow strip close to or far from the boundary). Note that with zero-flux boundary conditions, packet waves may transform into standing waves (see also [12]) after reflection from the boundary.

What are the properties of packet waves? First, a single wave cannot exist alone. Waves emerge at one end and disappear at the other end of the wave packet (see Figs. 1a and 3a), which slowly expands and can occupy the entire medium after a very long period of time (thousands of oscillation periods).

Packet waves have small amplitude. Consider the reduced Eq. (1) with $\beta = s = 0$ at constant z. For fz small

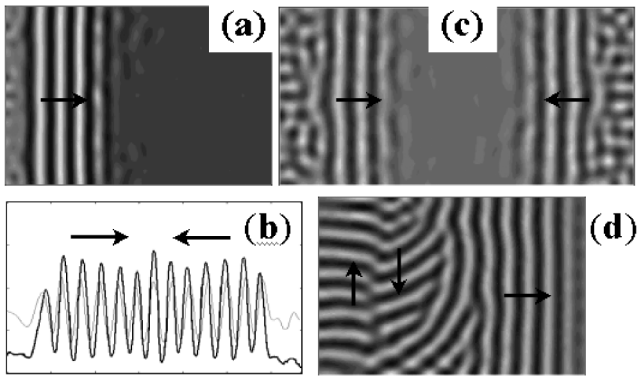

FIG. 3. Computer simulation of Eqs. (1)–(4) for positive dispersion $d\omega_k/dk$ in cases (a1) (a) and (b2) (b)–(d). (a),(d) Size = 150 × 100, (c) size = 200 × 100. Narrow ($L/100$, $L = 150$) left vertical stripe was perturbed in (a) and (d). (b) Concentration profile along the horizontal line [continuation of (c)] at time ($t = 500$) when two packets collide. In (b) dark (light) line corresponds to activator (catalyst).

$[q/(3 - 8^{1/2}) < fz \ll 1$; $q/(3 - 8^{1/2})$ is the minimum value of fz that gives bistability], the equation has two stable (x_1 and x_3) and one unstable (x_2) steady states, with $q < x_1 < x_2 < x_3 < 1$; $x_2 \cong fz - q$, $x_3 \cong 1$. Trigger waves have an amplitude of about x_3, or at least significantly larger than x_2. In our case, x oscillates around the steady state of the full system (1)–(4), $x_{SS} \cong q(f + 1)/(f - 1 + q)$, which is close to x_2. Collision of two wave packets leads to an increase in the amplitude of oscillations at the point (line) of collision (see Fig. 3b), in contrast to the behavior of trigger waves.

The dark and light stripes in our packet waves have approximately equal widths, reflecting the fact that at each spatial point we have nearly sinusoidal rather than relaxation oscillations.

The velocity of waves within a packet, ν_{pw}, which is actually a phase velocity, is given by

$$\nu_{\mathrm{pw}} = \omega_0/k_0 \,. \tag{5}$$

Although the velocities of packet and phase waves have the same dependence on ω_0 and k_0, the velocity of packet waves depends on the diffusion coefficients, and packet waves are unable to pass through an impermeable barrier as phase waves can. The velocity ν_{pw} significantly exceeds the velocity of the trigger front, ν_{tf}, in the corresponding bistable subsystem:

$$\partial x/\partial\tau = [x - x^2 - k_{\mathrm{out}}(x - q)/(x + q) - \beta x + s]/\varepsilon + D_x\Delta x \,, \tag{1r}$$

$$\partial s/\partial\tau = (\beta x - s)/\varepsilon_1 + D_s\Delta s \,, \tag{3r}$$

where the pseudorate constant k_{out} replaces fz. When $k_{\mathrm{out}} \cong q/(3 - 8^{1/2})$, ν_{tf} reaches its maximum. We then obtain in case (a1) $k_0 \cong 0.61$, $\omega_0 \cong 1.01$, and $\nu_{\mathrm{pw}} \cong 1.7$, while $\nu_{\mathrm{tf}} = 1.005$. In case (c3), $k_0 \cong 0.955$, $\omega_0 \cong 1.27$, $\nu_{\mathrm{pw}} \cong 1.33$, and $\nu_{\mathrm{tf}} = 0.7566$. The velocity of the wave packet (group velocity) depends, in general, on $|d\omega_k/dk|$ and is significantly smaller than ω_0/k_0 in the cases considered here.

In cases (b2) and (d4), when $a_k < 0$, the final patterns are standing waves like those shown in Fig. 4d. In the former case, the transient period from initial perturbation to final pattern may be as long as several thousand oscillation periods, depending on the shape of the initial perturbation, the geometry of the reaction area, and the parameters of the system. During the transient period, we observed irregular waves enveloped by packets of plane waves (Fig. 3c) like those in the experiment shown in Fig. 1b. In this computer simulation, two identical narrow vertical strips adjacent to the left and right borders were slightly perturbed. First, a packet of plane waves developed. Then, after several hundred oscillation periods T, irregular, broken waves emerged near the boundaries (no flux boundary conditions). The wave patterns from the left and right sides

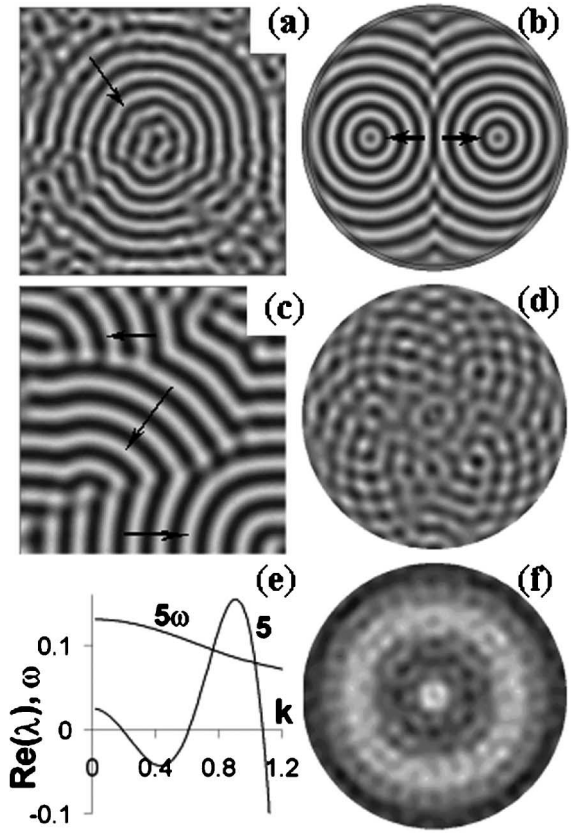

FIG. 4. Computer simulation of Eqs. (1)–(4) for negative dispersion $d\omega_k/dk$. Dispersion curves for simulations (a), (d), and (f) correspond to cases (c3), (d4), and Fig. (4e), respectively. Dispersion curve for simulations (b) and (c) is similar to that of cases (c3), but with slightly different parameters: (c),(e) $q = 0.0033$, (c),(e) $f = 1.3$, (c) $\varepsilon = 0.383$, (e) $\varepsilon = 0.384$, (c),(e) $\varepsilon_1 = 3.25$, (c),(e) $\varepsilon_2 = 0.001\,15$, (c),(e) $\alpha = 12$, (c),(e) $\beta = 0.3$, (c),(e) $\gamma = 0.15$, (c),(e) $\chi = 0.003\,575$, (c),(e) $D_x = D_z = 0.015$, (c),(e) $D_u = 1$, (c) $D_s = 0.8$, (e) $D_s = 0.6$. (a) Size = 100 × 100, (b),(f) $R = 50$, (c) size = 60 × 60, (d) $R = 60$. (a),(d),(f) perturbation at center, (b) two points symmetric about center (at $x = \pm R/2$) were perturbed, (c) random initial conditions.

were not identical, though the initial perturbations were the same.

For case (b2), we also obtained traveling waves moving in opposite directions in adjacent areas (Fig. 3d), as in the experiment in Fig. 1c. Initially, a narrow vertical strip was perturbed at the left side. As in Fig. 3c, a packet of plane waves developed, followed by chaotic waves. After several hundred T, new plane waves moving in opposite directions evolved from the irregular waves, while the initial wave packet shifted to the right (Fig. 3d). Note the similarity between the experiments shown in Figs. 1b and 1c and the simulations presented in Figs. 3c and 3d.

The behavior of system (1)–(4) when $d\omega_k/dk < 0$ is shown in Fig. 4. Negative dispersion (which was found only for $\chi \neq 0$) combined with Hopf instability ($a_k > 0$ at $k = 0$) gives rise to inwardly propagating waves that move toward the point (line) of perturbation. In the BZ-AOT system, when antispirals occur, the frequency of bulk oscillations, f_{bo}, is larger than the frequency of antispirals, f_{as}, i.e., $\omega_H \equiv \omega_{k=0} > \omega_0$, as in the case of negative dispersion. Propagating concentric waves that can transform into inwardly rotating spirals have been obtained for a point perturbation (Fig. 4a). When we perturbed at two points (Fig. 4b), we obtained accelerating waves emerging between two wave basins, as seen in experiments on antispirals [7]. When a vertical wave between two basins splits, two new waves move in opposite directions, and other waves from above and below rush into the free space left by these waves, because each point of the oscillatory medium is oscillating at frequency ω_0. These accelerating waves may thus be regarded as phase waves and may have very high velocity, while the velocity of plane waves within a packet is determined by Eq. (5). With random initial conditions, we find waves with negative curvature and the centers of their arcs situated at the boundary (cf. simulation in Fig. 4c and experiment in Fig. 1d).

To examine the mechanism of formation of packet waves we explored model parameters that yield the dispersion curves shown in Fig. 4e. There is a band of k at which $a_k < 0$, while $a_k > 0$ in bands at smaller and at larger k. In this case, we find (Fig. 4f) two separate, overlapping patterns: small (0.002) amplitude standing waves with short wavelength ($l \cong 7.3$) and large (0.013) amplitude phase waves with long wavelength ($l \cong 30$), oscillating about a mean concentration x of about 0.087. The standing waves maintain their shape and frequency during propagation of the phase waves. This simulation suggests that inwardly propagating packet waves arise from bulk oscillations (positive a_k at $k = 0$), and then the mechanism of mode selection chooses the wavelength with maximum a_k if and only if $a_k > 0$ between $k = 0$ and $k = k_0$.

To assess whether the sign of $d\omega/dk$ at $k = k_0$ or the difference, $\omega_H - \omega_0$, between the frequencies of bulk and local oscillations determines the direction of wave propagation, we performed the simulations shown in Figs. 2b–2d. In both cases (1) and (2) in Fig. 2b, $\omega_H - \omega_0 > 0$, but the signs of $d\omega/dk$ differ. We see that inwardly propagating waves occur only when $d\omega/dk < 0$.

We have focused here mainly on cases when the group velocity is significantly smaller than the velocity of packet waves. However, the opposite situation can also occur. If $d\omega_k/dk \cong \omega_0/k_0 > 0$, outwardly propagating packet waves are replaced by a single solitonlike wave. A more interesting situation can arise when $d\omega_k/dk$ is negative and $|d\omega_k/dk| \cong \omega_0/k_0$. When $|d\omega_k/dk| \ll \omega_0/k_0$, individual waves within a packet appear to propagate from a sink to the source. Causality is not violated, however, since the *packet* of waves propagates outward. If $|d\omega_k/dk| \cong \omega_0/k_0$, the initial perturbation may be trapped in the form of local oscillations, and wave propagation may be inhibited. This important case, potentially useful for building a chemical memory, will be studied separately in future work. Also, a more general treatment of packet waves in the context of Ginzburg-Landau equations would be extremely useful.

The agreement between the experiments and the simulations suggests that our model reflects the key features of this system. The finite wavelength instability gives rise to packets with a well defined velocity, ω_0/k_0, for plane waves. If, in addition, $d\omega_k/dk < 0$ at the characteristic wave number k_0, the familiar outwardly propagating waves are transformed to the inwardly propagating waves found in the BZ-AOT system in the form of antispirals and antipacemakers [7]. To our knowledge, this Letter presents the first observation of packet waves in a reaction-diffusion system.

This work was supported by the Chemistry Division of the National Science Foundation. We thank Anatol Zhabotinsky for helpful discussions.

[1] E. Ben-Jacob, I. Cohen, and H. Levine, Adv. Phys. **49**, 395 (2000).
[2] M. C. Cross and P. C. Hohenberg, Rev. Mod. Phys. **65**, 851 (1993).
[3] J. P. Gollub and J. S. Langer, Rev. Mod. Phys. **71**, s396 (1999).
[4] K. J. Lee, Phys. Rev. Lett. **79**, 2907 (1997).
[5] A. T. Winfree, Science **175**, 634 (1972).
[6] A. N. Zaikin and A. M. Zhabotinsky, Nature (London) **225**, 535 (1970).
[7] V. K. Vanag and I. R. Epstein, Science **294**, 835 (2001).
[8] D. Balasubramanian and G. A. Rodley, J. Phys. Chem. **92**, 5995 (1988).
[9] V. K. Vanag and I. Hanazaki, J. Phys. Chem. **99**, 6944 (1995).
[10] V. K. Vanag and I. R. Epstein, Phys. Rev. Lett. **87**, 228301 (2001).
[11] J. P. Keener and J. J. Tyson, Physica (Amsterdam) **21D**, 307 (1986).
[12] A. M. Zhabotinsky, M. Dolnik, and I. R. Epstein, J. Chem. Phys. **103**, 10 306 (1995).